ACS APPLIED MATERIALS & INTERFACES

www.acsami.org

Research Article

Air-Derived Inhibitor of Nanozymes

Tong Li, Qi Mei, Yuting Wang, Qi Sun, Shujie Liu, Yihong Zhang, Wanling Liu, Gen Wei, Min Zhou, and Hui Wei*

Cite This: *ACS Appl. Mater. Interfaces* 2023, 15, 28421−28429

Read Online

ACCESS | Metrics & More | Article Recommendations | Supporting Information

ABSTRACT: Nanozymes are functional nanomaterials with enzyme-mimicking activities, which have found wide applications in various fields. Investigation on nanozyme inhibitors not only helps to apply nanozymes in a controlled manner but also deepens our insight into the catalysis mechanism. Herein, we report an inorganic ion inhibitor, HCO_3^-, which can significantly inhibit the alkaline phosphatase-mimicking activities of Ce_6 cluster-based metal−organic framework (Ce-MOF) nanozymes. The inhibition of adsorption of the negatively charged fluorescence sodium on Ce_6 clusters in Ce-MOF nanoparticles (NPs) by HCO_3^- proves that HCO_3^- ions occupy and deactivate Ce_6 clusters (i.e., catalytic active sites), leading to the activity inhibition of Ce-MOF nanozymes. Tris(hydroxymethyl)aminomethane hydrochloride (Tris−HCl) buffer is widely employed as the alkaline reaction medium. HCO_3^- ions can be formed in Tris−HCl buffer through adsorption of CO_2 in the air during storage in a sealed tube, which significantly inhibits the activity of Ce-MOF nanozymes. To our knowledge, this study is the first to demonstrate an air-derived inhibitor of nanozymes.

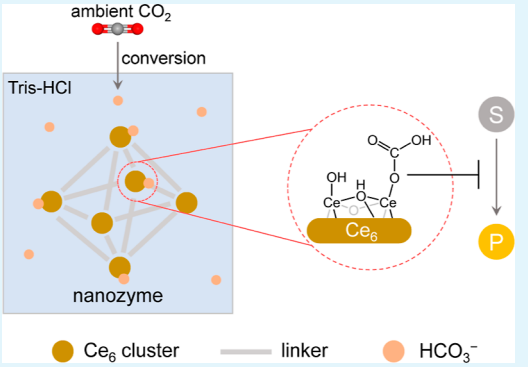

KEYWORDS: *nanozymes, inhibitors, HCO_3^-, Ce-MOF, air*

INTRODUCTION

Nanozymes are functional nanomaterials with enzyme-mimicking activities, which have found wide applications in the fields of bioanalysis,[1−5] diagnosis,[6,7] therapeutics,[8−10] agriculture,[11,12] and environmental protection.[13,14] Nanozymes possess several advantages, including low cost, easy fabrication, and good stability, but the moderate activity of nanozymes compared with their natural counterparts has restricted their further development.[15−19] Considerable efforts have been devoted to the rational design and synthesis of highly active nanozymes.[20−23] It is also essential to achieve their best activities during the employment of nanozymes. Similar to natural enzymes, inhibitors can weaken the activities of nanozymes, resulting in poor application performance.[24,25] Study of nanozyme inhibitors not only helps to realize their maximal activities but also guarantees their optimal application performances.

Over the last several years, some inorganic ions, small molecules, and macromolecules have been reported to serve as inhibitors of peroxidase/oxidase-mimicking nanozymes, leading to decreased activities.[26] In general, some of the reported inhibitors are target analytes.[24,27] Other inhibitors have been added by scientists for the design of "turn-off−turn-on" sensors.[28,29] For hydrolytic nanozymes, phosphate ions or phosphate derivatives have been widely reported to significantly inhibit their activities.[30] An interesting study reported that the product, dimethyl phosphate, formed during the hydrolysis of dimethyl 4-nitrophenylphosphate catalyzed by Zr_6 cluster-based metal−organic frameworks (Zr-MOFs) can inhibit the activity of Zr-MOFs, as dimethyl phosphate can occupy and deactivate the catalytic sites (i.e., Zr_6 clusters).[31] Basically, all of the reported inhibitors are derived from solutions. It has rarely been reported that ambient air can also result in the formation of inhibitors, which further deactivate nanozymes insensibly, leading to underestimated activities and inferior application performances of nanozymes.

Herein, we report a unique inorganic ion inhibitor, HCO_3^-, which could be formed in a widely used alkaline buffer, tris(hydroxymethyl)aminomethane hydrochloride (Tris−HCl), through adsorption of CO_2 in the air even in a sealed tube. For alkaline phosphatase, its inhibitors, phosphate ions, compete with substrates in binding to the catalytic active sites (Figure 1a). Similar to alkaline phosphatase, HCO_3^- can serve as an inhibitor of Ce_6 cluster-based MOF (Ce-MOF) nanozymes by occupying and deactivating the catalytic active sites (i.e., Ce_6 clusters) (Figure 1b). This study demonstrates an air-derived inhibitor of alkaline phosphatase-mimicking

Received: May 1, 2023
Accepted: May 23, 2023
Published: May 31, 2023

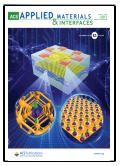

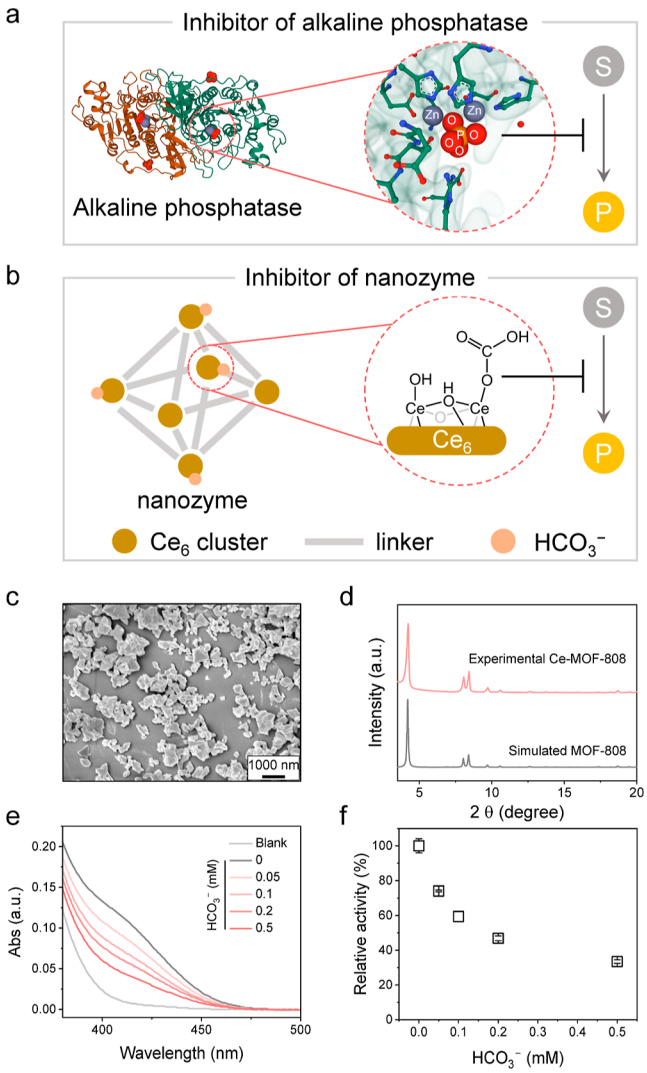

Figure 1. Inhibition of the alkaline phosphatase-mimicking activity of Ce-MOF-808 NPs by HCO_3^-. (a) Schematic illustration of activity inhibition of an alkaline phosphatase by phosphate ions. (b) Schematic illustration of inhibition of the phosphatase-mimicking activity of a Ce-MOF nanozyme by HCO_3^-. (c) Representative SEM image of Ce-MOF-808 NPs. (d) XRD patterns of Ce-MOF-808 NPs and simulated MOF-808. (e) UV−vis spectra of 0.5 mM *b*NPP before and after a 10 min incubation with 200 μg/mL Ce-MOF-808 NPs in the presence of HCO_3^- at varying concentrations. (f) Influence of HCO_3^- concentration on the relative activity of Ce-MOF-808 NPs. Data are expressed as the mean ± standard error of three experiments.

nanozymes and will offer us an insight into the activity measurements and applications of nanozymes.

RESULTS AND DISCUSSION

Phosphate ions are inhibitors of alkaline phosphatase.[32,33] We first monitored the influence of HPO_4^{2-} concentration on the activity of alkaline phosphatase. As expected, the activity of alkaline phosphatase decreased with increasing concentrations of added HPO_4^{2-} (Figure S1). Ce_6 cluster-based MOF (Ce-MOF) NPs are well known for their alkaline phosphatase-mimicking activities, and Ce_6 clusters serve as catalytic active centers.[34−37] We first chose Ce-MOF-808 NPs as our study model, which were fabricated as reported.[38] As shown in Figure 1c, the experimental Ce-MOF-808 NPs exhibited an irregular morphology. The X-ray diffraction (XRD) pattern of the experimental Ce-MOF-808 NPs corresponded well to the simulated MOF-808, which indicated the successful synthesis of Ce-MOF-808 NPs (Figure 1d). The catalytic reaction was carried out in Tris−HCl buffer with a pH of 8.0. We first proved the stability of Ce-MOF-808 NPs in the reaction medium. The supernatant of Ce-MOF-808 NPs in Tris−HCl buffer exhibited no catalytic activity, proving that the catalytic activity came from Ce-MOF-808 NPs rather than possibly released cerium species (Figure S2). Ce-MOF-808 NPs after soaking in the reaction medium exhibited identical XRD patterns to the simulated MOF-808, indicating their intact crystal structures (Figure S3). The activity of Ce-MOF-808 NPs remained unchanged after three weeks of storage, demonstrating their good storage stability (Figure S4). We then monitored the influence of HCO_3^- concentration on the alkaline phosphatase-mimicking activity of Ce-MOF-808 NPs. As shown in Figure 1e,f, the activity of Ce-MOF-808 NPs was lowered when the HCO_3^- concentration increased. A relatively low HCO_3^- concentration of 0.2 mM inhibited half of the activity of Ce-MOF-808 NPs.

In addition to Ce-MOF-808 NPs, we also fabricated three other Ce-MOF NPs, including Ce-MOF-801 NPs, Ce-UiO-66 NPs, and Ce-UiO-67 NPs. As shown in Figure 2a, SEM images showed that the three Ce-MOF NPs exhibited irregular morphologies. The XRD patterns of the three Ce-MOF NPs corresponded well to their simulated counterparts, proving the successful fabrication of NPs. Furthermore, we monitored the influence of HCO_3^- concentration on the alkaline phosphatase-mimicking activities of Ce-MOF-801 NPs, Ce-UiO-66 NPs, and Ce-UiO-67 NPs. As expected, the increase of HCO_3^- concentration could significantly lower the catalytic activities of the three Ce-MOF NPs (Figures 2b−d and S5−S7). We speculate that HCO_3^- can occupy Ce_6 clusters in Ce-MOF NPs, which inhibits the substrate adsorption on Ce_6 clusters. Hence, HCO_3^- can decrease the alkaline phosphatase-mimicking activity of not only Ce-MOF-808 NPs but also other Ce-MOF NPs, including Ce-MOF-801 NPs, Ce-UiO-66 NPs, and Ce-UiO-67 NPs. We also monitored the influence of HCO_3^- on the alkaline phosphatase-like activity of CeO_2. It was shown that the addition of HCO_3^- could also inhibit the activity of CeO_2, although not as significantly as Ce-MOF NPs (Figure S8).

Before verifying the deactivation of Ce_6 clusters by HCO_3^-, we first excluded the possible influence of HCO_3^- addition on the pH of the reaction medium. The absorbance of the reaction product, *p*-nitrophenol (*p*NP), was pH-dependent. When the pH decreased, the absorbance of *p*NP at 407 nm also decreased (Figure S9). However, the addition of HCO_3^- did not change the absorbance of *p*NP (Figure S10). Therefore, the addition of HCO_3^- would not change the pH value of the Tris−HCl buffer adopted in the reaction. After exclusion of the possible influence of HCO_3^- on the reaction system pH, we then investigated the possible occupation of HCO_3^- on the Ce_6 clusters in Ce-MOF-808 NPs. Negatively charged dyes have been widely adsorbed by MOFs due to the interaction between functional groups such as the carboxyl groups of dyes and the metal nodes of MOFs.[39,40] Fluorescence sodium (FS) is a typical negatively charged dye containing carboxyl groups and phenol groups, which is supposed to be adsorbed on the Ce_6 clusters in Ce-MOF-808 NPs. We speculate that the addition of HCO_3^- could not only inhibit the adsorption of FS but also release the adsorbed FS on Ce_6 clusters (Figure 3a). As shown in Figure 3b, Ce-MOF-

https://doi.org/10.1021/acsami.3c06255
ACS Appl. Mater. Interfaces 2023, 15, 28421−28429

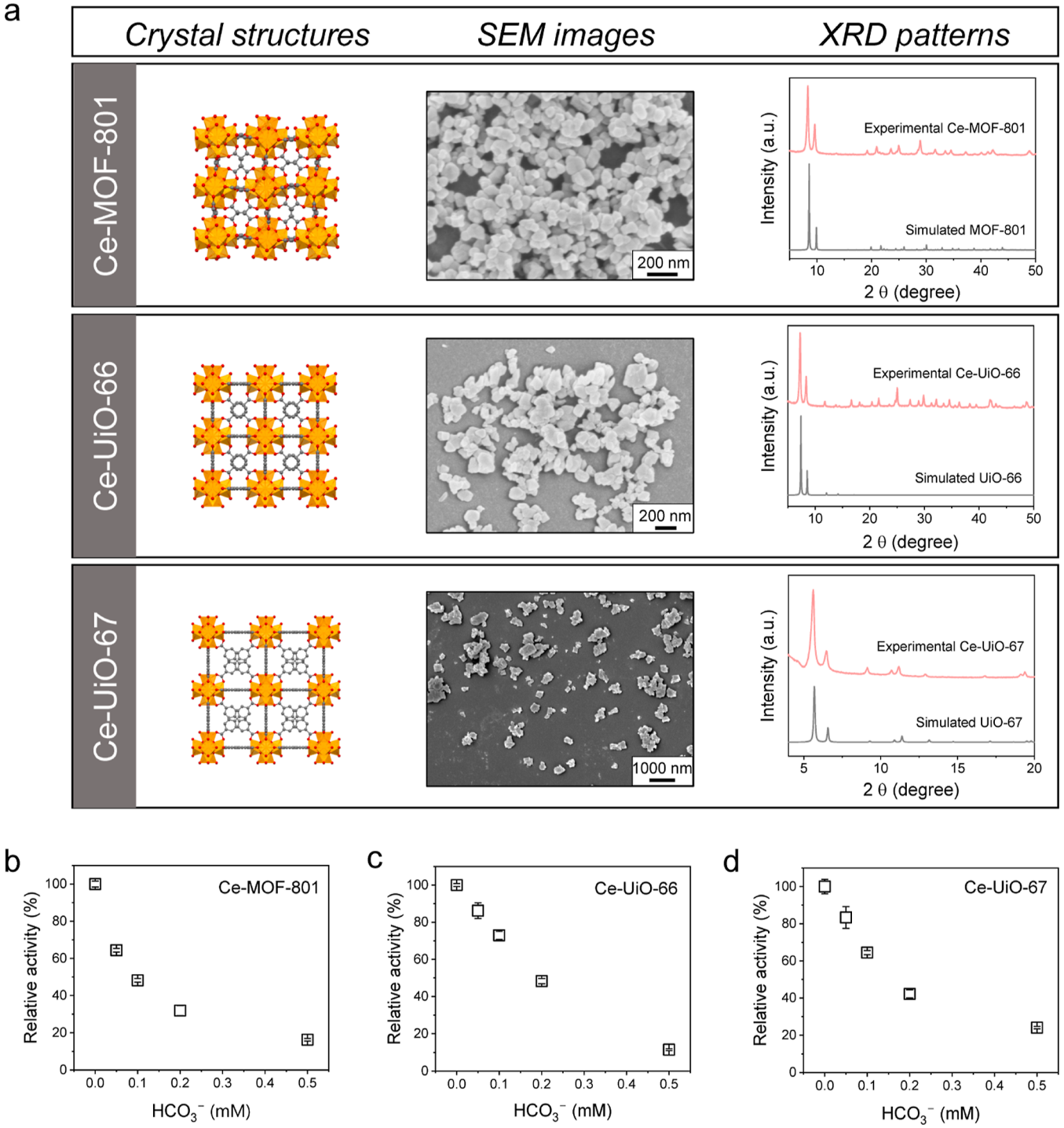

Figure 2. Inhibition of the alkaline phosphatase-mimicking activities of other Ce-MOF nanozymes by HCO_3^-. (a) Crystal structures, representative SEM images, and XRD patterns of the other three Ce-MOF NPs. UV−vis spectra of *b*NPP after incubation with (b) Ce-MOF-801 NPs, (c) Ce-UiO-66 NPs, and (d) Ce-UiO-67 NPs in the presence of HCO_3^- with varying concentrations. Data are expressed as mean ± standard error of three experiments.

808 NPs exhibited a yellow color after incubation with FS, while a green color was found in the presence of HCO_3^-. We further added HCO_3^- into the suspension containing Ce-MOF-808 NPs and FS, and the color of the suspension turned from yellow to green. Besides, the addition of HCO_3^- did not change the color of Ce-MOF-808 NPs or FS (Figures S11 and S12). The phenomenon demonstrated that HCO_3^- might compete against FS in binding to Ce_6 clusters in Ce-MOF-808 NPs.

FS has an absorption peak at 490 nm. We further monitored the UV−vis spectra of Ce-MOF-808 NPs and FS with or without HCO_3^-. It was shown that the presence of HCO_3^- led to a higher absorbance at 490 nm compared with the absence of HCO_3^-. Furthermore, the additional introduction of HCO_3^- could recover the absorbance of Ce-MOF-808 NPs and FS at 490 nm to almost the same value as those in the presence of HCO_3^- (Figure 3c,d). We also monitored the fluorescent intensity at 525 nm of Ce-MOF-808 NPs and FS

https://doi.org/10.1021/acsami.3c06255
ACS Appl. Mater. Interfaces 2023, 15, 28421−28429

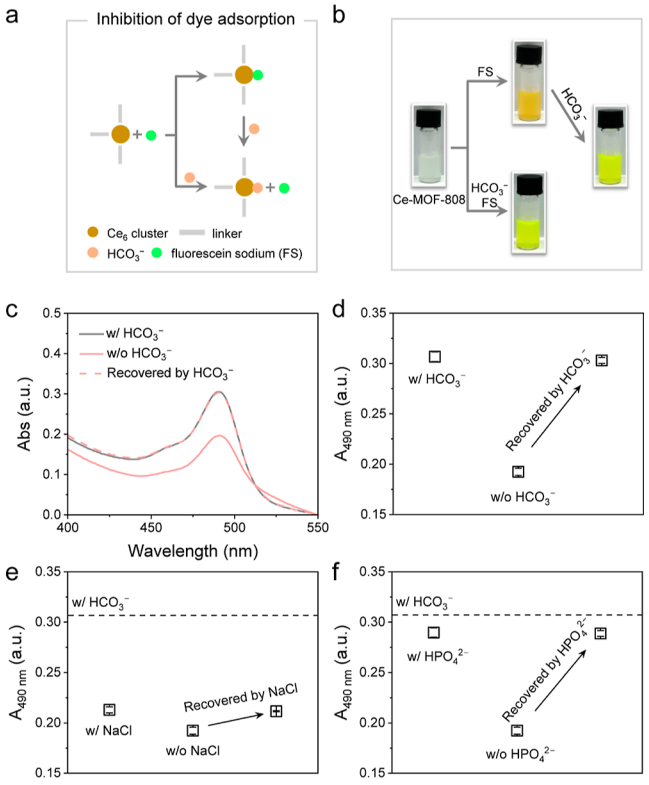

Figure 3. Inhibition of fluorescein sodium (FS) adsorption on Ce_6 clusters in Ce-MOF-808 NPs by HCO_3^-. (a) Schematic illustration of inhibition of FS adsorption on Ce_6 clusters by HCO_3^-. (b) Photos of Ce-MOF-808 NPs in Tris−HCl buffer before and after incubation with FS, HCO_3^- and FS, and FS followed by the addition of HCO_3^-. (c) UV−vis spectra of Ce-MOF-808 NPs and FS after 2 min incubation with or without 1 mM HCO_3^- and recovered by 1 mM HCO_3^-. (d) Absorbance values at 490 nm ($A_{490\ nm}$) corresponding to panel c. (e) $A_{490\ nm}$ of UV−vis spectra of Ce-MOF-808 NPs and FS after 2 min incubation with or without 1 mM NaCl and recovered by 1 mM NaCl. (f) $A_{490\ nm}$ of UV−vis spectra of Ce-MOF-808 NPs and FS after 2 min incubation with or without 0.2 mM HPO_4^{2-} and recovered by 0.2 mM HPO_4^{2-}. Data are expressed as the mean ± standard error of three experiments.

with or without HCO_3^-. An identical trend was demonstrated (Figure S13). The results indicated that HCO_3^- competed with FS in binding to Ce_6 clusters. When HCO_3^- was absent, FS occupied Ce_6 clusters, leading to a lower absorbance at 490 nm, which might be ascribed to two possible reasons. One reason is that Ce-MOF-808 NPs could scatter the incident light so that FS in Ce-MOF-808 NPs could not absorb the light. The other reason might be that the lone electron pair of FS occupies the d orbital of Ce in Ce_6 clusters, leading to a lower absorbance at 490 nm. To figure out the reason, we directly incubated Ce^{4+} with FS in the absence or presence of HCO_3^-. We found that the presence of HCO_3^- also led to a higher absorbance of Ce^{4+} and FS at 490 nm compared with the absence of HCO_3^- (Figure S14). As expected, HCO_3^- could also inhibit the alkaline phosphatase-mimicking activity of Ce^{4+} (Figure S15). Hence, it was speculated that the presence of HCO_3^- can break the interaction between FS and Ce_6 clusters, thus leading to a higher absorbance at 490 nm. To exclude the potential influence of increased ionic strength caused by HCO_3^-, we studied the inhibition of FS adsorption by employing NaCl with an identical concentration to that of HCO_3^-. Different from HCO_3^-, the presence of NaCl could not significantly lead to a higher absorbance value at 490 nm compared with the absence of NaCl (Figures 3e and S16a). It is widely known that phosphate ions can bind to metal nodes in MOFs.[41] We studied the inhibition of FS adsorption using HPO_4^{2-}. Similar to HCO_3^-, the presence of HPO_4^{2-} could also result in a much higher absorbance at 490 nm compared with the absence of HPO_4^{2-}. In addition, the additional introduction of HPO_4^{2-} could also recover the absorbance at 490 nm (Figures 3f and S16b). Hence, it was expected that HPO_4^{2-} could also significantly inhibit the activity of Ce-MOF-808 NPs (Figures S17 and S18). Overall, HCO_3^- could bind to Ce_6 clusters, inhibiting the alkaline phosphatase-mimicking activities of Ce-MOF NPs.

The hydrolysis reaction catalyzed by MOFs is usually performed under mild basic conditions. Tris−HCl buffer is an ideal choice because of its buffering range of 7.0−9.0. However, Tris−HCl is very prone to adsorb CO_2 from the air. We speculate that HCO_3^- could be formed in Tris−HCl buffer after exposure to air, which could inhibit the alkaline phosphatase-mimicking activity of Ce-MOF NPs (Figure 4a). To prove our hypothesis, we directly exposed Tris−HCl buffer with a pH of 8.0 to air. After 1 day of exposure, we adopted Tris−HCl buffer as the reaction medium to measure the activity of Ce-MOF-808 NPs. Exposure to the air of Tris−HCl buffer significantly lowered the activity of Ce-MOF-808 NPs by approximately 70% (Figure 4b,c). In addition to Ce-MOF-808 NPs, exposure to the air of Tris−HCl buffer could also significantly decrease the activities of Ce-MOF-801 NPs, Ce-UiO-66 NPs, and Ce-UiO-67 NPs (Figures S19−S21). To prove the formation of HCO_3^- in Tris−HCl buffer after exposure to air, we adopted the $CaCO_3$ precipitation method. We exposed a Tris solution containing $CaCl_2$ with a pH of 10.9 to the air under stirring for 1 day. We observed the formation of white precipitates (Figure 4d). The precipitate was confirmed to be calcite, a kind of $CaCO_3$ crystal, by XRD and SEM images (Figure 4e,f). The results indicated the formation of CO_3^{2-} in Tris solution at pH 10.9. According to the Bjerrum plot of H_2CO_3, it is supposed that HCO_3^- could be formed in Tris−HCl buffer with pHs of 8.0−9.0 (Figure S22). We also speculate that exposure of Tris−HCl buffer to the air sealed in a vessel such as a centrifuge tube could also form HCO_3^-, which inhibits the activity of Ce-MOF NPs. We employed a 50 mL centrifuge tube in which different volumes of Tris−HCl buffer were added, and parafilm was further used to seal the tube (Figure 4g). The volume of the tube used in our hand is around 57 mL. By controlling the volume of the added Tris−HCl buffer, the air volume in the sealed tube can be finely tuned. When 50 mL of Tris−HCl buffer was sealed in the tube and stored for 1 day, there was no activity inhibition of Ce-MOF-808 NPs. However, when the ratio of air volume to buffer volume increased from 32/25 to 52/5, a significant decrease in the activity was demonstrated (Figure 4h,i). The inhibition effect was enhanced with an increase in the air volume in the sealed tube. Not only was the activity of Ce-MOF-808 NPs inhibited using Tris−HCl buffer after exposure to air in the sealed tube, but the activities of Ce-MOF-801 NPs, Ce-UiO-66 NPs, and Ce-UiO-67 NPs were also decreased (Figures S23−S25). It is widely known that the content of the greenhouse gas CO_2 in the atmosphere has been increasing gradually over the last several decades. A recent paper shows that the ambient CO_2 content is around 410 ppm.[42] Hence, the calculated ambient CO_2 molar concentration is around 18.3 μM. Assuming that CO_2 in the sealed

https://doi.org/10.1021/acsami.3c06255
ACS Appl. Mater. Interfaces 2023, 15, 28421−28429

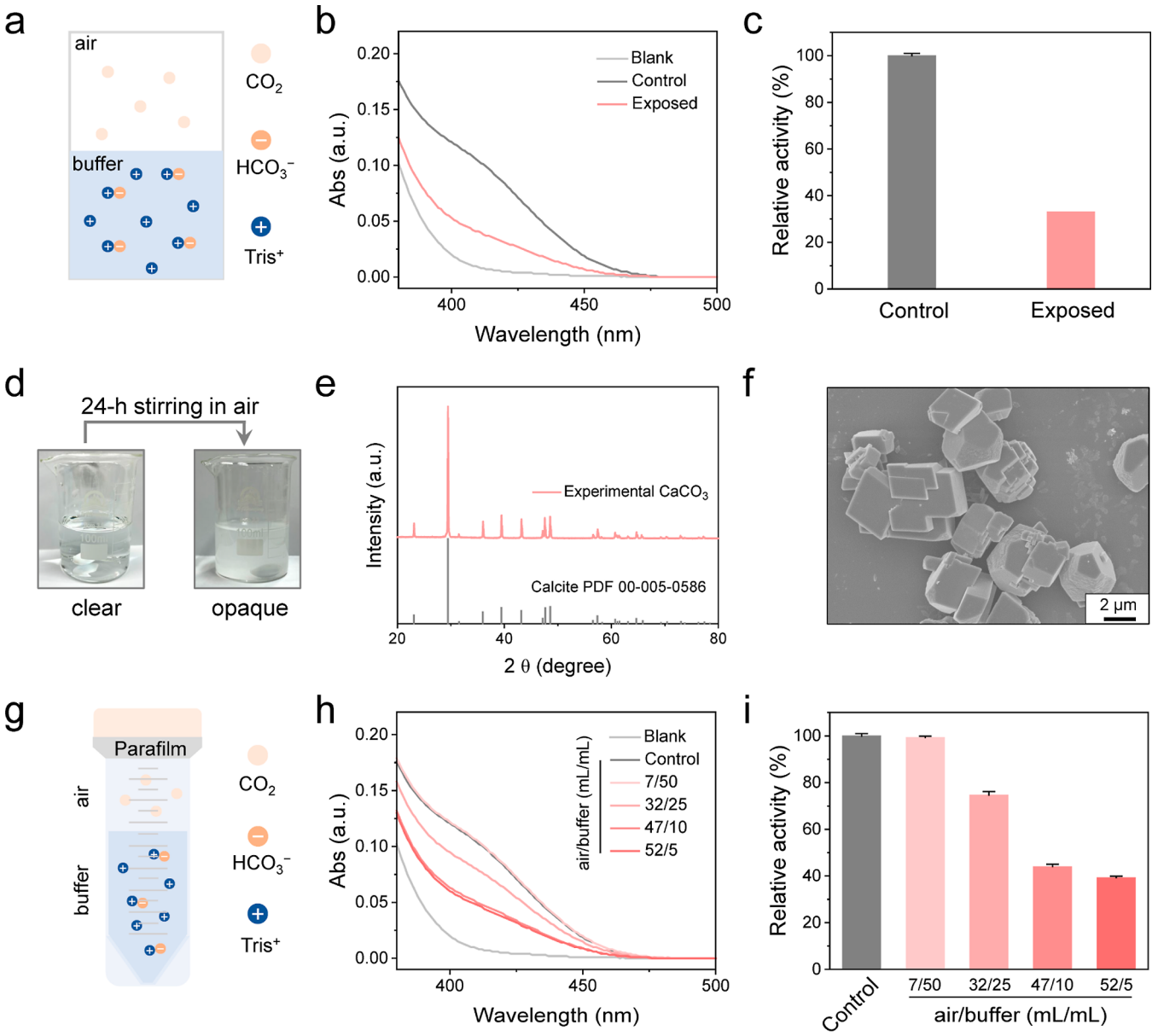

Figure 4. Inhibition of the alkaline phosphatase-mimicking activity of Ce-MOF-808 NPs by CO_2 adsorption in Tris−HCl buffer. (a) Schematic illustration of HCO_3^- formation in Tris−HCl buffer after exposure to air. (b) UV−vis spectra of 0.5 mM *b*NPP after 10 min incubation with 200 μg/mL Ce-MOF-808 NPs in 0.2 M Tris−HCl buffer with a pH of 8.0 before and after 1 day of exposure to air. (c) Influence of exposure to air on the relative activity of Ce-MOF-808 NPs. (d) Photographs of 0.2 M Tris in the presence of 20 mM $CaCl_2$ with a pH of 10.9 before and after 1 day exposure to air under stirring, showing the formation of $CaCO_3$. (e) XRD patterns of the formed $CaCO_3$ and simulated calcite. (f) Representative SEM image of the formed $CaCO_3$. (g) Schematic illustration of HCO_3^- formation in Tris−HCl buffer in a parafilm-sealed tube. (h) UV−vis spectra of 0.5 mM *b*NPP after 10 min incubation with 200 μg/mL Ce-MOF-808 NPs in 0.2 M Tris−HCl buffer with a pH of 8.0 after 1 day exposure to air with varying volumes in a parafilm-sealed tube. (i) Influence of the air volume in the tube on the relative activity of Ce-MOF-808 NPs. Data are expressed as the mean ± standard error of three experiments.

tube was fully converted to HCO_3^- in Tris−HCl buffer, we estimated that when the ratio of air volume to buffer volume increased, the HCO_3^- concentration increased rapidly (Figure S26). Notably, when the ratio increased to 52/5, around 0.2 mM HCO_3^- could be formed in the buffer, a concentration, which could significantly inhibit the activity of Ce-MOF NPs. The result demonstrated above reminded us that the air volume in the sealed tube storing Tris−HCl buffer should be controlled to a relatively low value to avoid the formation of HCO_3^-, which inhibits the alkaline phosphatase-mimicking activities of Ce-MOF NPs.

CONCLUSIONS

In summary, we have reported an air-derived inhibitor, HCO_3^-, which can significantly inhibit the alkaline phosphatase-mimicking activities of Ce-MOF nanozymes. The inhibition effect mainly came from the occupation and deactivation of the catalytic active sites, i.e., Ce_6 clusters, by HCO_3^-, according to an FS adsorption inhibition experiment. A widely employed alkaline buffer, Tris−HCl, was found to adsorb CO_2 easily from the air in the sealed tube during storage, leading to the formation of HCO_3^-, which significantly inhibited the activities of Ce-MOF nanozymes. It was

https://doi.org/10.1021/acsami.3c06255
ACS Appl. Mater. Interfaces 2023, 15, 28421−28429

reminded that the air in the sealed vessel storing Tris−HCl buffer should be controlled as little as possible. We speculate that this study will broaden our insight into the inhibitors of nanozymes.

EXPERIMENTAL SECTION

Chemicals and Reagents. Diammonium cerium(IV) nitrate [$(NH_4)_2Ce(NO_3)_6$], acetic acid, tris(hydroxymethyl)aminomethane (Tris), hydrogen chloride (HCl), dimethylformamide (DMF), sodium phosphate dibasic dodecahydrate ($Na_2HPO_4{\cdot}12H_2O$), sodium bicarbonate ($NaHCO_3$), sodium chloride (NaCl), dimethyl sulfoxide (DMSO), acetone, formic acid, FS, calcium chloride ($CaCl_2$), and *p*-nitrophenol (*p*NP) were bought from Sinopharm Chemical Reagent Co., Ltd. Trimesic acid, fumaric acid, terephthalic acid, and 4,4′-biphenyldicarboxylic acid were bought from Aladdin. Alkaline phosphate from porcine kidney was bought from Sigma. Disodium *p*-nitrophenyl phosphate (*p*NPP) was bought from Bidepharm. Sodium bis(4-nitrophenyl) phosphate (*b*NPP) was bought from Meryer. Ultrapure water (18 $M\Omega{\cdot}cm^{-1}$) was obtained from a Milli-Q purification system.

Fabrication of Ce-MOF NPs. For Ce-MOF-808 NPs, in a typical procedure,[38] $(NH_4)_2Ce(NO_3)_6$ (470 mg) was dissolved in 1.6 mL of water in a 50 mL flask. The solution was heated at 100 °C in an oil bath for 5 min under stirring, followed by the introduction of 5.85 mL of acetic acid. The solution was further heated for 5 min at 100 °C. Trimesic acid (60 mg) was dissolved in 4.8 mL of DMF, which was added into the flask dropwise. The solution was heated at 100 °C for 1 h under stirring. After cooling down to room temperature, Ce-MOF-808 NPs were obtained by centrifugation and washed with DMF three times over a total period of 24 h. Ce-MOF-808 NPs were further washed with acetone once, soaked in acetone overnight, and dried under vacuum.

For Ce-MOF-801 NPs, in a typical procedure,[37] fumaric acid (870 mg) was added to a 50 mL beaker. $(NH_4)_2Ce(NO_3)_6$ (470 mg) was dissolved in 13.868 mL of water and 1.132 mL of formic acid. The solution was poured into the beaker under stirring. After a 10 min reaction, Ce-MOF-801 NPs were obtained by centrifugation and washed with DMF three times over a total period of 24 h. Ce-MOF-801 NPs were further washed with acetone once, soaked in acetone overnight, and dried under vacuum.

For Ce-UiO-66 NPs, in a typical procedure,[43] $(NH_4)_2Ce(NO_3)_6$ (1.17 g) was dissolved in 4 mL of water and 244 μL of acetic acid in a 30 mL vial. The vial was heated at 60 °C for 30 min in an oven, which was further cooled down at 4 °C in a refrigerator. Terephthalic acid (355 mg) was dissolved in 18.76 mL of DMF and added to the vial. The vial was further heated at 80 °C for 30 min. After cooling down to room temperature, Ce-UiO-66 NPs were obtained by centrifugation and washed with DMF three times over a total period of 24 h. Ce-UiO-66 NPs were further washed with acetone once, soaked in acetone overnight, and dried under vacuum.

For Ce-UiO-67 NPs, in a typical procedure, $(NH_4)_2Ce(NO_3)_6$ (585 mg) was dissolved in 2 mL of water and 122 μL of acetic acid in a 10 mL vial. The vial was heated at 60 °C for 30 min in an oven, which was further cooled down at 4 °C in a refrigerator. 4,4′-Biphenyldicarboxylic acid (258 mg) was dispersed in 9.38 mL of DMF in a 50 mL flask and sonicated for 3 min. The $(NH_4)_2Ce(NO_3)_6$ solution in the vial was added to the flask, which was further heated at 80 °C for 45 min under stirring. After cooling down to room temperature, Ce-UiO-67 NPs were obtained by centrifugation and washed with DMSO four times over a total period of 24 h. Ce-UiO-66 NPs were further washed with acetone once, soaked in acetone overnight, and dried under vacuum.

Activity Inhibition of Alkaline Phosphatase. Typically, 5 μL of alkaline phosphate (20 U/mL) was added to 480 μL of Tris−HCl buffer with a pH of 9.0, followed by the addition of 10 μL of Na_2HPO_4 with varying concentrations (0, 10, 20, 50, and 100 mM). After 30 min of incubation at room temperature, 5 μL of 10 mM *p*NPP was added to initiate the reaction. After a 20 min reaction at room temperature, 200 μL of the reaction solution was placed into a 96-well plate, and the optical density at 407 nm was measured using a microplate reader.

Activity Inhibition of Ce^{4+}. Typically, 10 μL of 50 mM *p*NPP and 10 μL of $NaHCO_3$ with varying concentrations (0, 10, 25, 50, and 100 mM) were added into 470 μL of 0.2 M Tris−HCl buffer with a pH of 9.0. Then, 10 μL of 5 mg/mL $(NH_4)_2Ce(NO_3)_6$ was introduced to initiate the reaction. After a 10 min reaction, 200 μL of the reaction solution was placed into a 96-well plate, and the optical density at 407 nm was measured using a microplate reader.

Activity Inhibition of CeO_2. Bare CeO_2 nanozymes were fabricated according to a reported method.[44] For activity inhibition of CeO_2, typically 10 μL of 50 mM *p*NPP and 10 μL of $NaHCO_3$ with varying concentrations (0, 10, 25, 50, and 100 mM) were added into 475 μL of 0.2 M Tris−HCl buffer with a pH of 9.0. Then, 5 μL of 5 mg/mL CeO_2 was introduced to initiate the reaction. After 1 h of reaction, 200 μL of the reaction solution was placed into a 96-well plate, and the optical density at 407 nm was measured using a microplate reader.

Activity Inhibition of Ce-MOF NPs. For Ce-MOF-808 NPs, typically 20 μL of 25 mM *b*NPP (in DMSO) and 10 μL of $NaHCO_3$ with varying concentrations (0, 5, 10, 20, and 50 mM) were added into 950 μL of 0.2 M Tris−HCl buffer with a pH of 8.0. Then, 20 μL of 10 mg/mL Ce-MOF-808 NPs was introduced to initiate the reaction. After a 10 min reaction at room temperature, Ce-MOF-808 NPs were removed by centrifugation (13,000, 10 min), and 800 μL of the supernatant was taken for activity measurement using a spectrophotometer.

For Ce-MOF-801 NPs, typically 20 μL of 100 mM *b*NPP (in DMSO) and 10 μL of $NaHCO_3$ with varying concentrations (0, 5, 10, 20, and 50 mM) were added into 950 μL of 0.2 M Tris−HCl buffer with a pH of 9.0. Then, 20 μL of 10 mg/mL Ce-MOF-801 NPs was introduced to initiate the reaction. After a 20 min reaction at room temperature, Ce-MOF-801 NPs were removed by centrifugation (13,000, 10 min), and 800 μL of the supernatant was taken for activity measurement using a spectrophotometer.

For Ce-UiO-66 NPs, typically, 20 μL of 25 mM *b*NPP (in DMSO) and 10 μL of $NaHCO_3$ with varying concentrations (0, 5, 10, 20, and 50 mM) were added into 960 μL of 0.2 M Tris−HCl buffer with a pH of 8.0. Then, 10 μL of 10 mg/mL Ce-UiO-66 NPs was introduced to initiate the reaction. After 20 min reaction at room temperature, Ce-UiO-66 NPs were removed by centrifugation (13,000, 10 min), and 800 μL of the supernatant was taken for activity measurement using a spectrophotometer.

For Ce-UiO-67 NPs, typically 20 μL of 10 mM *b*NPP (in DMSO) and 10 μL of $NaHCO_3$ with varying concentrations (0, 5, 10, 20, and 50 mM) were added into 960 μL of 0.2 M Tris−HCl buffer with a pH of 9.0. Then, 10 μL of 10 mg/mL Ce-UiO-67 NPs (in DMSO) was introduced to initiate the reaction. After a 20 min reaction at room temperature, Ce-UiO-67 NPs were removed by centrifugation (13,000, 10 min), and 800 μL of the supernatant was taken for activity measurement using a spectrophotometer.

Stability Tests of Ce-MOF-808 NPs. To exclude the potential activity of the supernatant of Ce-MOF-808 NPs at pH 8.0, 20 μL of 10 mg/mL Ce-MOF-808 NPs was added into 980 μL of Tris−HCl buffer with a pH of 8.0. After 10 min of incubation, Ce-MOF-808 NPs were removed by centrifugation (13,000, 10 min), and 784 μL of the supernatant was taken, followed by the addition of 16 μL of 25 mM *b*NPP (in DMSO). After a 10 min reaction, the solution was measured using a spectrophotometer.

For storage stability, Ce-MOF-808 NPs (powder) in a tube were sealed and stored at room temperature for three weeks. The activity of Ce-MOF-808 NPs was measured before and after storage using the method mentioned above.

For XRD measurements, 20 mg Ce-MOF-808 NPs were soaked in 5 mL of Tris−HCl buffer with a pH of 8.0 for 1 h in the absence or presence of 10 mM $NaHCO_3$. After soaking, Ce-MOF-808 NPs were washed twice with water, twice with methanol, once with acetone, and soaked in acetone overnight. Ce-MOF-808 NPs were dried under vacuum before XRD measurements.

https://doi.org/10.1021/acsami.3c06255
ACS Appl. Mater. Interfaces 2023, 15, 28421−28429

pH-Dependent Absorbance of *p*NP. To investigate the influence of pH on the absorbance of *p*NP, 10 μL of 10 mM *p*NP (in DMSO) was added to 990 μL of 0.2 M buffer with a pH of 5.0, 7.4, or 9.0 (pH 5.0 acetic acid/sodium buffer, pHs 7.4 and 9.0 Tris−HCl buffer). The solution was further measured using a spectrophotometer.

Inhibition of FS Adsorption. Typically, 20 μL of 10 mg/mL Ce-MOF-808 NPs was added to 465 μL of 0.2 M Tris−HCl buffer, followed by the addition of 10 μL of water, 50 mM $NaHCO_3$, 50 mM NaCl, or 10 mM Na_2HPO_4. Then, 5 μL of 5 mM FS was introduced. After 2 min of incubation, the suspension was transferred to a cuvette with a light path of 1 mm and measured using a spectrophotometer.

For the recovery experiment, typically 20 μL of 10 mg/mL Ce-MOF-808 NPs was added into 465 μL of 0.2 M Tris−HCl buffer, followed by the addition of 5 μL of 5 mM FS. After 2 min of incubation, 10 μL of 50 mM $NaHCO_3$, or 50 mM NaCl, or 10 mM Na_2HPO_4 was added. After 2 min incubation, the suspension was transferred to a cuvette with a light path of 1 mm and measured using a spectrophotometer.

For the fluorescence measurement, 100 μL of the suspension after 2 min of incubation was placed into a 96-well plate. The fluorescent intensity at 525 nm was measured using a microplate reader with an excitation wavelength of 490 nm.

Inhibition of FS Absorbance by Ce^{4+}. Typically, 10 μL of 50 mM $(NH_4)_2Ce(NO_3)_6$ was added into 975 μL of 0.2 M Tris−HCl buffer with a pH of 8.0, followed by the addition of 10 μL of water or 50 mM $NaHCO_3$. Then, 5 μL of 2 mM FS was introduced. After 2 min of incubation, the solution was sonicated for seconds to dissolve possibly formed precipitated complexes and measured using a spectrophotometer.

For the recovery experiment, 10 μL of 50 mM $(NH_4)_2Ce(NO_3)_6$ was added into 975 μL of 0.2 M Tris−HCl buffer with a pH of 8.0, followed by the addition of 5 μL of 2 mM FS. After 2 min of incubation, 10 μL of 50 mM $NaHCO_3$ was added. After 2 min of incubation, the solution was sonicated for seconds to dissolve possibly formed precipitated complexes and measured using a spectrophotometer.

Storage of Tris−HCl Buffer. To investigate the influence of exposure to air on the alkaline phosphatase-mimicking activities of Ce-MOF NPs, 25 mL of Tris−HCl buffer with a pH of 8.0 or 9.0 was added into a 50 mL centrifuge tube. The tube was further placed at room temperature without a cap. After 1 day placement, the buffer was further employed for the activity measurements using the method mentioned above.

To investigate the influence of air volume in the sealed tube on the alkaline phosphatase-mimicking activities of Ce-MOF NPs, varying volumes of Tris−HCl buffer (5, 10, 25, 50 mL) with a pH of 8.0 or 9.0 were added into a 50 mL centrifuge tube with a cap sealed by parafilm. After 1 day placement, the buffer was further employed for the activity measurements using the method mentioned above. The 50 mL centrifuge tube used in our laboratory has a total volume of around 57 mL.

$CaCO_3$ Formation. To identify that Tris can adsorb CO_2 from air, forming carbonate species, 50 mL of 0.2 M Tris with a pH of 10.9 was added to a 100 mL beaker. $CaCl_2$ (110 mg) was introduced and dissolved in the beaker. After one day of stirring in air, the formed $CaCO_3$ was obtained by centrifugation and washed three times with water and three times with ethanol. After drying in vacuum, the obtained $CaCO_3$ was employed for XRD measurement.

Characterizations. The alkaline phosphatase-mimicking activities of Ce-MOF NPs, pH-dependent absorbance of *p*NP, stability tests of Ce-MOF-808, inhibition of FS adsorption, and inhibition of FS absorbance by Ce^{4+} were studied using a UV−vis spectrophotometer (UV-3600 Plus, Shimadzu). The activity inhibition of alkaline phosphatase, Ce^{4+}, CeO_2, and the fluorescence intensity of FS were studied using a microplate reader (SpectraMax M2e, Molecular Device). The morphology of Ce-MOF NPs and $CaCO_3$ was studied using a scanning electron microscope (Zeiss Ultra 55 microscope) at an acceleration voltage of 3 kV. The XRD patterns of Ce-MOF NPs and $CaCO_3$ were collected through a D8 ADVANCE diffractometer (Bruker) with a scanning rate of 3−5°/min.

■ ASSOCIATED CONTENT

Supporting Information

The Supporting Information is available free of charge at https://pubs.acs.org/doi/10.1021/acsami.3c06255.

Activity inhibition assay of alkaline phosphatase; storage stability of Ce-MOF-808 NPs; inhibition effect of HCO^{3-} on the activities of Ce-MOF NPs, CeO_2, and Ce^{4+}; influence of HCO_3^- on the pH of Tris−HCl buffer; influence of storage of Tris−HCl buffer on the activity of Ce-MOF NPs; and estimated formed HCO_3^- concentration in Tris−HCl buffer in a sealed tube (DOCX)

■ AUTHOR INFORMATION

Corresponding Author

Hui Wei − *Department of Biomedical Engineering, College of Engineering and Applied Sciences, Nanjing National Laboratory of Microstructures, Jiangsu Key Laboratory of Artificial Functional Materials, Nanjing University, Nanjing, Jiangsu 210023, China; State Key Laboratory of Analytical Chemistry for Life Science, School of Chemistry and Chemical Engineering, Chemistry and Biomedicine Innovation Center (ChemBIC), Nanjing University, Nanjing, Jiangsu 210023, China;* orcid.org/0000-0003-0870-7142; Email: weihui@nju.edu.cn

Authors

Tong Li − *Department of Biomedical Engineering, College of Engineering and Applied Sciences, Nanjing National Laboratory of Microstructures, Jiangsu Key Laboratory of Artificial Functional Materials, Nanjing University, Nanjing, Jiangsu 210023, China*

Qi Mei − *Department of Biomedical Engineering, College of Engineering and Applied Sciences, Nanjing National Laboratory of Microstructures, Jiangsu Key Laboratory of Artificial Functional Materials, Nanjing University, Nanjing, Jiangsu 210023, China*

Yuting Wang − *Department of Biomedical Engineering, College of Engineering and Applied Sciences, Nanjing National Laboratory of Microstructures, Jiangsu Key Laboratory of Artificial Functional Materials, Nanjing University, Nanjing, Jiangsu 210023, China*

Qi Sun − *Department of Biomedical Engineering, College of Engineering and Applied Sciences, Nanjing National Laboratory of Microstructures, Jiangsu Key Laboratory of Artificial Functional Materials, Nanjing University, Nanjing, Jiangsu 210023, China*

Shujie Liu − *Department of Biomedical Engineering, College of Engineering and Applied Sciences, Nanjing National Laboratory of Microstructures, Jiangsu Key Laboratory of Artificial Functional Materials, Nanjing University, Nanjing, Jiangsu 210023, China*

Yihong Zhang − *Department of Biomedical Engineering, College of Engineering and Applied Sciences, Nanjing National Laboratory of Microstructures, Jiangsu Key Laboratory of Artificial Functional Materials, Nanjing University, Nanjing, Jiangsu 210023, China*

Wanling Liu − *Department of Biomedical Engineering, College of Engineering and Applied Sciences, Nanjing National Laboratory of Microstructures, Jiangsu Key Laboratory of*

https://doi.org/10.1021/acsami.3c06255
ACS Appl. Mater. Interfaces 2023, 15, 28421−28429

Artificial Functional Materials, Nanjing University, Nanjing, Jiangsu 210023, China

Gen Wei − *Department of Biomedical Engineering, College of Engineering and Applied Sciences, Nanjing National Laboratory of Microstructures, Jiangsu Key Laboratory of Artificial Functional Materials, Nanjing University, Nanjing, Jiangsu 210023, China*

Min Zhou − *Department of Biomedical Engineering, College of Engineering and Applied Sciences, Nanjing National Laboratory of Microstructures, Jiangsu Key Laboratory of Artificial Functional Materials, Nanjing University, Nanjing, Jiangsu 210023, China*

Complete contact information is available at: https://pubs.acs.org/10.1021/acsami.3c06255

Notes

The authors declare no competing financial interest.

■ ACKNOWLEDGMENTS

This work was funded by the National Key R&D Program of China (2019YFA0709200 and 2021YFF1200700), the National Natural Science Foundation of China (21874067 and 21722503), the Jiangsu Provincial Key R&D Program (BE2022836), the PAPD Program, the CAS Interdisciplinary Innovation Team (JCTD-2020-08), and the Fundamental Research Funds for the Central Universities (021314380228, 202200325, and 021314380195).

■ REFERENCES

(1) Xi, Z.; Wei, K.; Wang, Q.; Kim, M. J.; Sun, S.; Fung, V.; Xia, X. Nickel-Platinum Nanoparticles as Peroxidase Mimics with a Record High Catalytic Efficiency. *J. Am. Chem. Soc.* **2021**, *143*, 2660−2664.

(2) Gao, L.; Zhuang, J.; Nie, L.; Zhang, J.; Zhang, Y.; Gu, N.; Wang, T.; Feng, J.; Yang, D.; Perrett, S.; Yan, X. Intrinsic Peroxidase-Like Activity of Ferromagnetic Nanoparticles. *Nat. Nanotechnol.* **2007**, *2*, 577−583.

(3) He, W.; Han, X.; Jia, H.; Cai, J.; Zhou, Y.; Zheng, Z. AuPt Alloy Nanostructures with Tunable Composition and Enzyme-like Activities for Colorimetric Detection of Bisulfide. *Sci. Rep.* **2017**, *7*, 40103.

(4) Zhao, J.; Gong, J.; Wei, J.; Yang, Q.; Li, G.; Tong, Y.; He, W. Metal Organic Framework Loaded Fluorescent Nitrogen-Doped Carbon Nanozyme with Light Regulating Redox Ability for Detection of Ferric Ion and Glutathione. *J. Colloid Interface Sci.* **2022**, *618*, 11−21.

(5) Liu, Q.; Wang, H.; Yang, Q.; Tong, Y.; He, W. Metal−Organic Frameworks Loaded Au Nanozymes with Enhanced Peroxidase-Like Activity for Multi-Targeted Biodetection. *Mater. Adv.* **2022**, *3*, 8557−8566.

(6) Broto, M.; Kaminski, M. M.; Adrianus, C.; Kim, N.; Greensmith, R.; Dissanayake-Perera, S.; Schubert, A. J.; Tan, X.; Kim, H.; Dighe, A. S.; Collins, J. J.; Stevens, M. M. Nanozyme-Catalysed CRISPR Assay for Preamplification-Free Detection of Non-coding RNAs. *Nat. Nanotechnol.* **2022**, *17*, 1120−1126.

(7) Ding, H.; Cai, Y.; Gao, L.; Liang, M.; Miao, B.; Wu, H.; Liu, Y.; Xie, N.; Tang, A.; Fan, K.; Yan, X.; Nie, G. Exosome-Like Nanozyme Vesicles for H_2O_2-Responsive Catalytic Photoacoustic Imaging of Xenograft Nasopharyngeal Carcinoma. *Nano Lett.* **2019**, *19*, 203−209.

(8) Sang, Y.; Cao, F.; Li, W.; Zhang, L.; You, Y.; Deng, Q.; Dong, K.; Ren, J.; Qu, X. Bioinspired Construction of a Nanozyme-Based H_2O_2 Homeostasis Disruptor for Intensive Chemodynamic Therapy. *J. Am. Chem. Soc.* **2020**, *142*, 5177−5183.

(9) Jana, D.; He, B.; Chen, Y.; Liu, J.; Zhao, Y. A Defect-Engineered Nanozyme for Targeted NIR-II Photothermal Immunotherapy of Cancer. *Adv. Mater.* **2022**, 2206401.

(10) Yang, J.; Zhang, R.; Zhao, H.; Qi, H.; Li, J.; Li, J. F.; Zhou, X.; Wang, A.; Fan, K.; Yan, X.; Zhang, T. Bioinspired Copper Single-Atom Nanozyme as a Superoxide Dismutase-Like Antioxidant for Sepsis Treatment. *Exploration* **2022**, *2*, 20210267.

(11) Zhao, L.; Bai, T.; Wei, H.; Gardea-Torresdey, J. L.; Keller, A.; White, J. C. Nanobiotechnology-Based Strategies for Enhanced Crop Stress Resilience. *Nat. Food* **2022**, *3*, 829−836.

(12) Gong, J.; Liu, Q.; Cai, L.; Yang, Q.; Tong, Y.; Chen, X.; Kotha, S.; Mao, X.; He, W. Multimechanism Collaborative Superior Antioxidant CDzymes to Alleviate Salt Stress-Induced Oxidative Damage in Plant Growth. *ACS Sustainable Chem. Eng.* **2023**, *11*, 4237−4247.

(13) Li, S.; Hou, Y.; Chen, Q.; Zhang, X.; Cao, H.; Huang, Y. Promoting Active Sites in MOF-Derived Homobimetallic Hollow Nanocages as a High-Performance Multifunctional Nanozyme Catalyst for Biosensing and Organic Pollutant Degradation. *ACS Appl. Mater. Interfaces* **2020**, *12*, 2581−2590.

(14) Natalio, F.; Andre, R.; Hartog, A. F.; Stoll, B.; Jochum, K. P.; Wever, R.; Tremel, W. Vanadium Pentoxide Nanoparticles Mimic Vanadium Haloperoxidases and Thwart Biofilm Formation. *Nat. Nanotechnol.* **2012**, *7*, 530−535.

(15) Zhang, R.; Yan, X.; Fan, K. Nanozymes Inspired by Natural Enzymes. *Acc. Mater. Res.* **2021**, *2*, 534−547.

(16) Huang, Y.; Ren, J.; Qu, X. Nanozymes: Classification, Catalytic Mechanisms, Activity Regulation, and Applications. *Chem. Rev.* **2019**, *119*, 4357−4412.

(17) Jiang, D.; Ni, D.; Rosenkrans, Z. T.; Huang, P.; Yan, X.; Cai, W. Nanozyme: New Horizons for Responsive Biomedical Applications. *Chem. Soc. Rev.* **2019**, *48*, 3683−3704.

(18) Wei, H.; Gao, L.; Fan, K.; Liu, J.; He, J.; Qu, X.; Dong, S.; Wang, E.; Yan, X. Nanozymes: A Clear Definition with Fuzzy Edges. *Nano Today* **2021**, *40*, 101269.

(19) Fan, K.; Gao, L.; Wei, H.; Jiang, B.; Wang, D.; Zhang, R.; He, J.; Meng, X.; Wang, Z.; Fan, H.; Wen, T.; Duan, D.; Chen, L.; Jiang, W.; Lu, Y.; Jiang, B.; Wei, Y.; Li, W.; Yuan, Y.; Dong, H.; Zhang, L.; Hong, C.; Zhang, Z.; Cheng, M.; Geng, X.; Hou, T.; Hou, Y.; Li, J.; Tang, G.; Zhao, Y.; Zhao, H.; Zhang, S.; Xie, J.; Zhou, Z.; Ren, J.; Huang, X.; Gao, X.; Liang, M.; Zhang, Y.; Xu, H.; Qu, X.; Yan, X. Nanozymes. *Prog. Chem.* **2023**, *35*, 1−87.

(20) Wei, Y.; Wu, J.; Wu, Y.; Liu, H.; Meng, F.; Liu, Q.; Midgley, A. C.; Zhang, X.; Qi, T.; Kang, H.; Chen, R.; Kong, D.; Zhuang, J.; Yan, X.; Huang, X. Prediction and Design of Nanozymes Using Explainable Machine Learning. *Adv. Mater.* **2022**, *34*, 2201736.

(21) Wang, X.; Gao, X. J.; Qin, L.; Wang, C.; Song, L.; Zhou, Y. N.; Zhu, G.; Cao, W.; Lin, S.; Zhou, L.; Wang, K.; Zhang, H.; Jin, Z.; Wang, P.; Gao, X.; Wei, H. e_g Occupancy as an Effective Descriptor for the Catalytic Activity of Perovskite Oxide-Based Peroxidase Mimics. *Nat. Commun.* **2019**, *10*, 704.

(22) Wang, Z.; Wu, J.; Zheng, J. J.; Shen, X.; Yan, L.; Wei, H.; Gao, X.; Zhao, Y. Accelerated Discovery of Superoxide-Dismutase Nanozymes via High-Throughput Computational Screening. *Nat. Commun.* **2021**, *12*, 6866.

(23) Xi, Z.; Cheng, X.; Gao, Z.; Wang, M.; Cai, T.; Muzzio, M.; Davidson, E.; Chen, O.; Jung, Y.; Sun, S.; Xu, Y.; Xia, X. Strain Effect in Palladium Nanostructures as Nanozymes. *Nano Lett.* **2020**, *20*, 272−277.

(24) Wu, W.; Huang, L.; Zhu, X.; Chen, J.; Chao, D.; Li, M.; Wu, S.; Dong, S. Reversible Inhibition of the Oxidase-Like Activity of Fe Single-Atom Nanozymes for Drug Detection. *Chem. Sci.* **2022**, *13*, 4566−4572.

(25) Xu, Y.; Xue, J.; Zhou, Q.; Zheng, Y.; Chen, X.; Liu, S.; Shen, Y.; Zhang, Y. The Fe-N-C Nanozyme with Both Accelerated and Inhibited Biocatalytic Activities Capable of Accessing Drug-Drug Interactions. *Angew. Chem., Int. Ed.* **2020**, *59*, 14498−14503.

(26) Chang, Y.; Gao, S.; Liu, M.; Liu, J. Designing Signal-on Sensors by Regulating Nanozyme Activity. *Anal. Methods* **2020**, *12*, 4708−4723.

(27) Weerathunge, P.; Ramanathan, R.; Torok, V. A.; Hodgson, K.; Xu, Y.; Goodacre, R.; Behera, B. K.; Bansal, V. Ultrasensitive

Colorimetric Detection of Murine Norovirus Using Nanozyme Aptasensor. *Anal. Chem.* **2019**, *91*, 3270−3276.
(28) Chang, Y.; Liu, M.; Liu, J. Highly Selective Fluorescent Sensing of Phosphite through Recovery of Poisoned Nickel Oxide Nanozyme. *Anal. Chem.* **2020**, *92*, 3118−3124.
(29) Wang, X.; Jiang, X.; Wei, H. Phosphate-responsive 2D-Metal−Organic-Framework-Nanozymes for Colorimetric Detection of Alkaline Phosphatase. *J. Mater. Chem. B* **2020**, *8*, 6905−6911.
(30) Liu, H.; Liu, J. Self-Limited Phosphatase-Mimicking CeO_2 Nanozymes. *ChemNanoMat* **2020**, *6*, 947−952.
(31) Liao, Y.; Sheridan, T.; Liu, J.; Farha, O.; Hupp, J. Product Inhibition and the Catalytic Destruction of a Nerve Agent Simulant by Zirconium-Based Metal−Organic Frameworks. *ACS Appl. Mater. Interfaces* **2021**, *13*, 30565−30575.
(32) Upadhyay, L. S. B.; Verma, N. Alkaline Phosphatase Inhibition Based Conductometric Biosensor for Phosphate Estimation in Biological Fluids. *Biosens. Bioelectron.* **2015**, *68*, 611−616.
(33) Fernley, H. N.; Walker, P. G. Studies on Alkaline Phosphatase. Inhibition by Phosphate Derivatives and the Substrate Specificity. *Biochem. J.* **1967**, *104*, 1011−1018.
(34) Bhattacharjee, S.; Chakraborty, T.; Bhaumik, A. A Ce-MOF as an Alkaline Phosphatase Mimic: Ce-OH_2 Sites in Catalytic Dephosphorylation. *Inorg. Chem. Front.* **2022**, *9*, 5735−5744.
(35) Loosen, A.; Simms, C.; Smolders, S.; De Vos, D. E.; Parac-Vogt, T. N. Bimetallic Ce/Zr UiO-66 Metal−Organic Framework Nanostructures as Peptidase and Oxidase Nanozymes. *ACS Appl. Nano Mater.* **2021**, *4*, 5748−5757.
(36) Islamoglu, T.; Atilgan, A.; Moon, S.-Y.; Peterson, G. W.; DeCoste, J. B.; Hall, M.; Hupp, J. T.; Farha, O. K. Cerium (IV) vs Zirconium (IV) Based Metal−Organic Frameworks for Detoxification of a Nerve Agent. *Chem. Mater.* **2017**, *29*, 2672−2675.
(37) Li, S.; Zhou, Z.; Tie, Z.; Wang, B.; Ye, M.; Du, L.; Cui, R.; Liu, W.; Wan, C.; Liu, Q.; Zhao, S.; Wang, Q.; Zhang, Y.; Zhang, S.; Zhang, H.; Du, Y.; Wei, H. Data-Informed Discovery of Hydrolytic Nanozymes. *Nat. Commun.* **2022**, *13*, 827.
(38) Liu, Y.; Li, H.; Liu, W.; Guo, J.; Yang, H.; Tang, H.; Tian, M.; Nie, H.; Zhang, X.; Long, W. Design of Monovalent Cerium-Based Metal Organic Frameworks as Bioinspired Superoxide Dismutase Mimics for Ionizing Radiation Protection. *ACS Appl. Mater. Interfaces* **2022**, *14*, 54587−54597.
(39) Jia, S.; Song, S.; Zhao, X. Selective Adsorption and Separation of Dyes from Aqueous Solution by a Zirconium-Based Porous Framework Material. *Appl. Organomet. Chem.* **2021**, *35*, No. e6314.
(40) Haque, E.; Jun, J. W.; Jhung, S. H. Adsorptive Removal of Methyl Orange and Methylene Blue from Aqueous Solution with a Metal−Organic Framework Material, Iron Terephthalate (MOF-235). *J. Hazard. Mater.* **2011**, *185*, 507−511.
(41) Yang, J.; Dai, Y.; Zhu, X.; Wang, Z.; Li, Y.; Zhuang, Q.; Shi, J.; Gu, J. Metal−Organic Frameworks with Inherent Recognition Sites for Selective Phosphate Sensing through Their Coordination-Induced Fluorescence Enhancement Effect. *J. Mater. Chem. A* **2015**, *3*, 7445−7452.
(42) Zhu, C.; Langley, J. A.; Ziska, L. H.; Cahoon, D. R.; Megonigal, J. P. Accelerated Sea-Level Rise is Suppressing CO_2 Stimulation of Tidal Marsh Productivity: A 33-year Study. *Sci. Adv.* **2022**, *8*, No. eabn0054.
(43) Yang, J.; Li, K.; Li, C.; Gu, J. Intrinsic Apyrase-Like Activity of Cerium-Based Metal-Organic Frameworks (MOFs): Dephosphorylation of Adenosine Tri- and Diphosphate. *Angew. Chem., Int. Ed.* **2020**, *59*, 22952−22956.
(44) Zhao, S.; Li, Y.; Liu, Q.; Li, S.; Cheng, Y.; Cheng, C.; Sun, Z.; Du, Y.; Butch, C. J.; Wei, H. An Orally Administered CeO_2@ Montmorillonite Nanozyme Targets Inflammation for Inflammatory Bowel Disease Therapy. *Adv. Funct. Mater.* **2020**, *30*, 2004692.

https://doi.org/10.1021/acsami.3c06255
ACS Appl. Mater. Interfaces 2023, 15, 28421−28429